

Article

Direct Production of Ferrochrome by Segregation Reduction of Chromite in the Presence of Calcium Chloride

Dawei Yu *  and Dogan Paktunc * 

CanmetMINING, Natural Resources Canada, 555 Booth Street, Ottawa, ON K1A 0G1, Canada

* Correspondence: dawei.yu@hotmail.com (D.Y.); dogan.paktunc@canada.ca (D.P.);

Tel.: +1-613-947-8024 (D.Y.); +1-613-947-7061 (D.P.)

Received: 20 December 2017; Accepted: 16 January 2018; Published: 19 January 2018

Abstract: A solid reduction process is described whereby chromite is reduced with the help of calcium chloride to produce ferrochrome alloy powders with high metal recovery. The process involves segregation reduction of chromite using graphite as the reductant and calcium chloride as the segregation catalyst. Experiments were performed in the temperature range of 1200–1400 °C to evaluate the influences of various design parameters using both a thermogravimetric analyzer and an electric tube furnace with continuous off-gas analysis. The reduced products were characterized by scanning electron microscopy, X-ray powder diffraction, synchrotron X-ray absorption spectroscopy, and were subjected to wet chemical analysis. It was concluded that the addition of calcium chloride not only accelerated the carbothermic reduction of chromite but also promoted the formation and growth of individual ferrochrome alloy particles. The alloy formation within chromite particles was minimized, enabling the effective separation of ferrochrome alloy particles from the unwanted gangue without the need for fine grinding. Majority of the calcium chloride remained in a recoverable form, with a small percentage (<10 wt %) consumed by reacting with the siliceous gangue forming wadalite. Pure ferrochrome alloy powders were successfully produced with high metal recovery using elutriating separation.

Keywords: chromite; ferrochrome; carbothermic reduction; segregation; CaCl₂; elutriation

1. Introduction

Ferrochromium, which is a critical alloy in the production of stainless steel and high-alloying ferritic steel [1], has been produced worldwide by carbothermic smelting reduction of chromite in submerged electric arc furnaces (SAF) for almost a century [2,3]. More than 90% of the high carbon ferrochrome produced, with a typical composition range of 60–70 wt % Cr, 6–8 wt % C and <5 wt % Si [1], is used for stainless steel production. The SAF process for ferrochrome production is extremely electric energy-intensive [3], with the specific energy consumption (SEC) in the range of 2.4–4.8 MWh per ton of ferrochrome produced [4]. Among the various SAF smelting technologies, pre-reduction of chromite before SAF smelting generally results in a lower SEC, because significant amounts of energy that are required for both heating the feed material and for enabling the endothermic reduction reactions are supplied by burning fuels in the pre-reduction stage, which is generally carried out in rotary kilns [5]. The premus process operates at a pre-reduction degree of ~50% Cr metallization, achieving a low SEC of 2.4 MWh/t [6].

As the most significant mineral source of Cr, chromite can be represented by the general formula $(\text{Mg,Fe}^{2+})(\text{Cr,Al,Fe}^{3+})_2\text{O}_4$ [7]. Reduction of chromite is relatively difficult due to its refractory nature, reflected partly by the strong oxygen bonding of the constituent cations. Unreduced cations (Mg^{2+} and Al^{3+}) can form a refractory product layer in the form of MgAl_2O_4

around unreduced or partially-reduced residual chromite, inhibiting further reduction [8]. In an effort to improve the carbothermic reduction kinetics of chromite, various fluxes were used as additives, such as CaO [9], SiO₂ [10–14], CaF₂ [15], combinations of NaF–CaF₂, fluorspar–feldspar–silica, and fluorspar–granite [16], etc. Many kinetic studies on the carbothermic reduction of chromite with/without the addition of fluxes [9,10,17–19] revealed that the ionic diffusion through the solid product layer could limit the reduction rate, due mainly to the presence of the unreducible oxides. Addition of some of the fluxes can accelerate the reduction rate by dissolving the solid refractory oxide layer forming molten slags.

Although significant research efforts have been made on the carbothermic solid reduction of chromite on the aspect of improving reduction kinetics, little attention was paid to alloy growth during solid reduction. The significance of alloy growth lies in the fact that it could potentially enable the direct production of pure ferrochrome by separation without the need of a SAF or a melting furnace for separating the alloy from the unwanted gangue/slag. Elimination of the SAF smelting or a melting operation means a much higher energy efficiency because the process will operate at the solid-state reduction regime of a much lower temperature. It can also remove the heavy reliance of the ferrochrome production on electric energy. Both of the two aspects bear much significance from the economic point of view.

From the perspectives of alloy growth during reduction and its subsequent separation, challenges arise due to the complexity of the carbothermic solid reduction mechanism. Metallic product inevitably formed in various regions of the reduction system, both inside or on the surface of the chromite phase [20], evidenced by the formation of significant amounts of fine alloy particles from both within chromite particles and on the surface [8,10,12,13,21]. A complex spatial relationship between the fine alloy particles and the unwanted materials in the reduced product means excessive grinding/milling is essential to physically liberate the alloy particles before separation (e.g., magnetic and gravitational separation). Excessive grinding of the reduced product not only consumes much electricity, but also likely produces powders too fine to be separable by conventional separation techniques. Therefore, the particle size of the ferrochrome alloys formed during reduction should be large enough to allow subsequent easy liberation and separation.

For the first time, we utilized the approach of segregation reduction of chromite with the use of CaCl₂ to prevent the alloy formation from within chromite particles while producing individual ferrochrome particles that are amenable for subsequent physical separation. Segregation phenomenon was accidentally discovered in the year 1923 when a particular Chilean copper ore was roasted with a solid fuel at 700 °C with the exclusion of oxygen [22]. Outward migration of the copper from finely-divided ore particles was observed. Further investigation revealed the key role of sodium chloride that was naturally present in the ore [22]. Subsequent extensive development led to the invention of the TORCO (Treatment of Refractory Copper Ores) process [23]. This segregation process incorporates four main steps [23]: (1) formation of HCl from the hydrolyzation of the salt by moisture in the presence of Si-bearing minerals; (2) formation of volatile cuprous chloride from the reaction between HCl and copper oxide; (3) generation of H₂ from reduction of water vapor by carbon; (4) reduction of cuprous chloride vapor in the vicinity of carbon particles by H₂, forming metallic copper and regenerating HCl. Segregation roasting has subsequently been studied to treat lateritic nickel ores [24–26] and iron ores [27,28].

The reasons for the choice of CaCl₂ as the segregation catalyst for chromite direct reduction include the following. First, CaCl₂ is readily available in large quantities because it is produced as a by-product of industrial processes [29,30]. Second, it is relatively cheap (300–400 USD/ton) [31]. Third, the boiling point of CaCl₂ is 1935 °C [32], indicating its potential for a low evaporation rate during chromite reduction at temperatures higher than 1200 °C. In comparison, the boiling point of NaCl is 1465 °C [32], meaning that significant evaporation would take place when using NaCl as the additive for chromite reduction.

2. Materials and Methods

2.1. Materials

The chromite ore from the Ring of Fire area of Northern Ontario was sieved to produce four size fractions used for the experiments. The average formula of chromite can be represented as $(\text{Mg}_{0.5}\text{Fe}_{0.5})(\text{Cr}_{1.4}\text{Fe}_{0.1}\text{Al}_{0.5})\text{O}_4$ [8]. Table 1 lists the compositions of the four size fractions of chromite. As shown, the finer size fractions contain higher amounts of the gangue minerals, evidenced by the lower Cr_2O_3 and higher SiO_2 concentrations. XRD (Rigaku D/MAX 2500, Rigaku Ltd., Tokyo, Japan) analysis of the 37–75 μm size fraction (Figure 1) indicates that the main gangue minerals are clinochlore ($(\text{Mg,Fe})_5\text{Al}(\text{Si}_3\text{Al})\text{O}_{10}(\text{OH})_8$), magnesite (MgCO_3), and phlogopite $\text{KMg}_3(\text{Si}_3\text{Al})\text{O}_{10}(\text{OH})_2$. Chromite size fraction of 180–300 μm has much less gangue, with only clinochlore identified by XRD (Figure 1). Flake-shaped graphite powders (99.9995% metal basis) were used as the reductant. Anhydrous calcium chloride (CaCl_2) was ground quickly in a mortar and pestle to a fine powder form before use, while minimizing moisture absorption.

Table 1. Chemical composition of the chromite of four size fractions.

Particle Size (μm)	Cr_2O_3	FeO *	MgO	Al_2O_3	SiO_2	TiO_2	V_2O_5	NiO	K_2O	CaO
37–75	35.32	15.92	18.51	10.42	9.79	0.21	0.18	0.29	0.44	0.17
75–105	44.36	19.71	14.07	10.84	4.54	0.27	0.20	0.17	0.21	0.09
105–180	46.42	20.50	12.85	11.16	3.35	0.28	0.19	0.12	0.10	0.06
180–300	47.36	20.92	12.71	11.61	2.95	0.28	0.22	0.10	0.06	0.04

* FeO: recast as total iron including a small fraction of Fe_2O_3 .

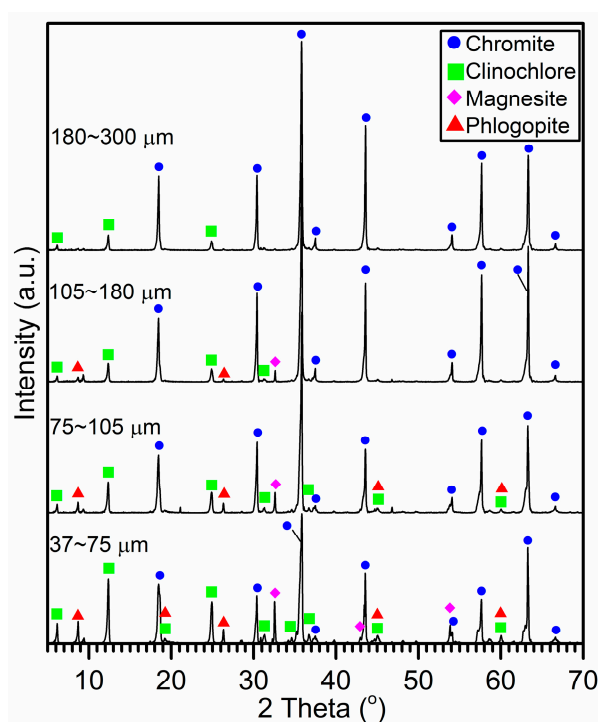


Figure 1. XRD patterns of the chromite ore of four size fractions.

2.2. Thermogravimetric Analysis

NETZSCH STA 449C Simultaneous Thermal Analyzer (Netzsch Gerätebau GmbH, Selb, Germany) coupled with a NETZSCH QMS 403 C Aeolos Mass Spectrometer was used for the thermogravimetric analysis (TG-DSC-MS). For each test, the ore sample, graphite and CaCl_2 with pre-determined mass proportions were homogenized before a pellet measuring 3 mm in diameter and approximately

70 mg in weight was prepared using a 3 mm die set. The pellet was placed in an alumina crucible (outer diameter 6.8 mm), and covered with an alumina lid (with one pin hole). The crucible was placed along with a reference crucible on the sample carrier before the measurement. A vacuum was applied to remove any residual air inside the TG-DSC chamber before a continuous flow of 100 mL/min Ar (5 N) was introduced. The sample was heated in the Ar flow at 20 °C/min to the target temperature, and dwell for 3 h before cooling down to room temperature.

2.3. Electric Tube Furnace Tests

The ore sample weighing 10 g was mixed with a pre-determined amount of graphite and CaCl₂ before pellets were prepared using a 13 mm die set. Each cylindrical pellet was approximately 2.5 g in weight, 13 mm in diameter, and about 15 mm in height. All pellets were placed in an alumina crucible (inner diameter 4 cm) before being placed inside the chamber of the vertical tube furnace. The samples were heated in an Ar flow of 500 mL/min at a rate of 6.25 °C/min to the target temperature for reduction. Samples were cooled as quickly as possible to room temperatures after 2 h dwell. The offgas was continuously measured for its CO and CO₂ concentrations by a gas analyzer (ABB EL3020, ABB, Cary, NC, USA).

2.4. Separation of Ferrochrome by Elutriating Tube

An elutriating tube similar to the one described by Frost [33] was used for the separation of ferrochrome from other unwanted materials in the reduced product, based on the density difference under a counter flow of water. A water pump with precise control of flowrate was used to continuously feed the water from the bottom of the elutriating tube. At a constant water flow after reaching steady state, denser particles were suspended in the lower and narrower section of the tube, while less dense particles were suspended in the upper and wider section. Separation was achieved by gradually lowering the water flowrate, causing only the alloy particles to settle to the bottom of the tube. The alloy particles were collected by discharging from the bottom into a receiver flask. The unwanted materials were also collected by stopping the water flow and discharging from the bottom of the tube.

2.5. Analytical Methods

As water-soluble CaCl₂ was present during reduction of chromite, quantification of the water-soluble species present in the reduced product was performed by water leaching of 1 g sample for 1 h, followed by filtration. The leachate was analyzed by inductively coupled plasma atomic emission spectrometry (ICP-AES, Varian VISTA RL, Varian, Palo Alto, CA, USA). Quantitative chemical analysis of solid samples was performed by completely dissolving the sample into aqueous solution using Na₂O₂ fusion technique, followed by analyzing the solution with ICP-AES. Polished sections of the reduced samples were prepared and examined by scanning electron microscopy (Hitachi S-3200N, Hitachi Corporation, Tokyo, Japan), which is coupled with an energy dispersive spectrometer (Quantax EDS, Bruker, Karlsruhe, Germany), with an accelerating voltage of 20 kV. Surface morphology of the reduced sample powders was also examined by firstly removing water-soluble chlorides with water leach, followed by filtration, and drying to remove moisture. The dried powders were then spread onto a double-sided carbon tape as a mono-layer, before SEM-EDS analysis. XRD analysis was performed using a Rigaku D/MAX 2500 (Rigaku Ltd., Tokyo, Japan) rotating-anode powder diffractometer with Cu K_α radiation at 40 kV, 200 mA.

X-ray absorption spectroscopy experiments were performed at the 9 BM and 20 BM beamlines of the Advanced Photon Source. Measurements were made on finely ground samples, spread onto tapes as monolayers. X-ray absorption spectra were collected by scanning the Si (111) monochromator in the 5780–6850 eV range (Cr K-edge) and 6911–7964 eV energy range (Fe K-edge). Samples were scanned four to five times in transmission and fluorescence modes using beam sizes of 1 mm × 1 mm and 1 mm × 2 mm. Chromium and iron foils were used for monitoring and calibrating energy shifts. Data reduction and analysis were made by ATHENA [34].

3. Results and Discussions

3.1. Effect of the Amount of CaCl_2

A series of isothermal TG-DSC-MS tests was firstly performed at 1300 °C using a mixture of chromite (75–105 μm), graphite (25–37 μm , 25 wt % of ore), and varying amount of CaCl_2 (0–30 wt % of ore). For each test, a 3 mm pellet was prepared from the mixture with a hydraulic press by employing a pressure of 200 MPa. The temperature profile, mass change (TG), heat flow (DSC), and gas analysis (MS) results are plotted in Figure 2. In order to allow direct comparison among the tests, each mass change curve (mg) was normalized to represent the test in which the starting sample contained exactly 50 mg chromite, 12.5 mg graphite, and varying amounts of CaCl_2 . As seen, the first thermal event took place at approximately 170 °C, represented by the sharp endotherm peak (DSC), H_2O peak, and the corresponding mass loss. Mass loss was absent in the test without CaCl_2 addition. This thermal event represents the evaporation of moisture which was initially absorbed by anhydrous CaCl_2 during preparation of the pellet. A second mass loss took place at approximately 570 °C, corresponding to the second H_2O peak. This was identified as the thermal dehydration of clinocllore. Detailed discussion on this thermal event can be found in our previous investigation [8]. A small endotherm at 761 °C resulted from the melting of CaCl_2 . The significant mass loss when the temperature reached 1300 °C was due to the carbothermic reduction of chromite, corresponding to an endotherm and the CO peaks. This can be represented by the much-simplified reaction Equation (1). A steeper mass loss and sharper CO peak can be observed at a higher CaCl_2 addition, indicating that the carbothermic reduction of chromite can be greatly accelerated in the presence of CaCl_2 .

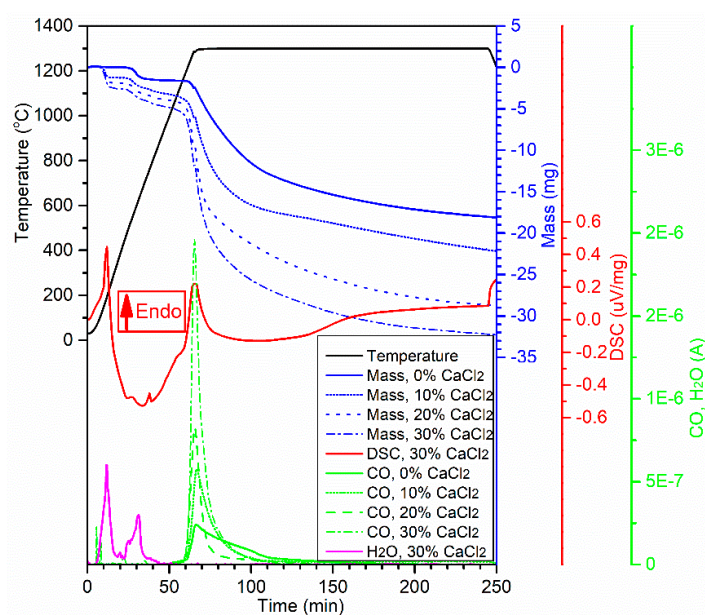


Figure 2. Isothermal thermogravimetric analysis (TG-DSC-MS) tests at 1300 °C, varying the amounts of CaCl_2 addition.

Figure 3 illustrates the cross sections of the reduced products. XRD patterns are shown in Figure 4 for comparison. In the absence of CaCl_2 (Figure 3a), each chromite particle was partially reduced, with a Cr-rich chromite core (light grey) and an outermost refractory spinel (MgAl_2O_4) layer (dark grey). The representative composition of the Cr-rich chromite core can be expressed as $(\text{Mg}_{0.95}\text{Fe}_{0.05})(\text{Cr}_{1.5}\text{Al}_{0.5})\text{O}_4$ based on semi-quantitative EDS microanalysis. Significant amounts of ferrochrome alloy particles were finely disseminated in each chromite particle, making it impossible

to recover by grinding for liberation followed by physical separation. The presence of residual chromite and appreciable amounts of graphite identified by XRD analysis (Figure 4) confirmed the incomplete chromite reduction in the absence of CaCl_2 . With the addition of 10 wt % CaCl_2 (Figure 3b), a much higher degree of reduction has taken place, evidenced by the absence of Cr-rich chromite cores. Most ferrochrome alloys formed outside of the original chromite particles due to the chloride segregation effect. Some small particles of Fe-rich ferrochrome alloy can still be observed inside the original chromite particles (e.g., the enlarged particle in Figure 3b). In the product resulted from 30 wt % CaCl_2 addition (Figure 3c), the completely reduced chromite particles are mainly composed of MgAl_2O_4 and MgO , and are nearly free of ferrochrome inclusions. Based on EDS analysis, the reduced chromite particles contain on average 1.1 wt % Cr and 0.1 wt % Fe, which translates to estimated metallization degrees of 98.9 wt % Cr and 99.8 wt % Fe. The individual ferrochrome alloy particles formed outside of the reduced chromite are mainly the M_7C_3 type carbide ($\text{M} = \text{Cr}, \text{Fe}$), with the Cr:Fe ratio determined by that of the starting chromite composition. In addition to carbide, MgAl_2O_4 , and MgO , XRD analysis (Figure 4) also identified wadalite ($\text{Ca}_6\text{Al}_5\text{Si}_2\text{O}_{16}\text{Cl}_3$) that resulted from the reaction of CaCl_2 with the silicate gangue (e.g., clinocllore) present in the ore, with the possible involvement of chromite.

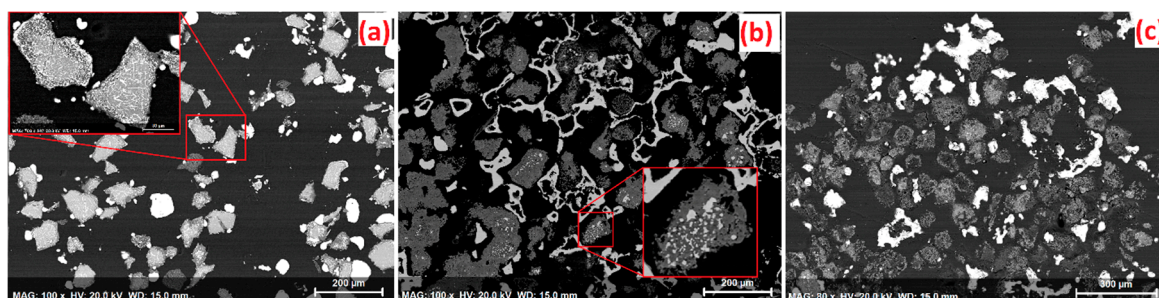


Figure 3. Backscattered electron micrographs of the reduced products from the tests with (a) no additive, (b) 10 wt %, and (c) 30 wt % CaCl_2 addition.

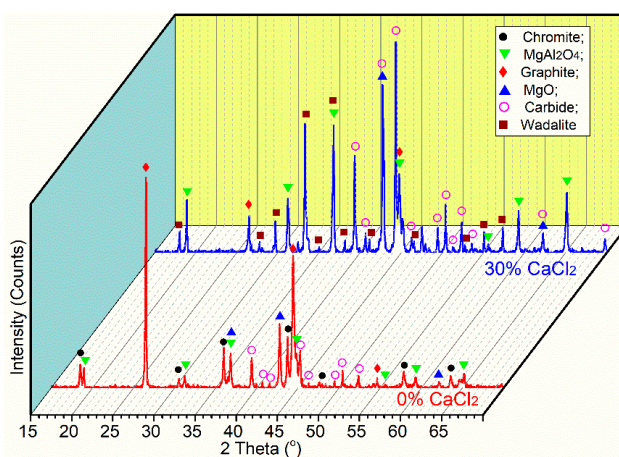


Figure 4. XRD patterns of the reduced products from the tests with no additive and 30 wt % CaCl_2 addition.

3.2. Effect of the Amount of Reductant

In theory, no less than the stoichiometric amount of carbonaceous reductant should be used in order to allow the complete the reduction of chromite. For example, the stoichiometric amount of carbon required for the complete reduction of the 75–105 μm chromite fraction, forming gaseous CO and M_7C_3 -type ferrochrome carbide is approximately 19 wt % of ore. In order to evaluate the

influence of excessive carbon on the reduction of chromite, electric tube furnace tests at 1300 °C were performed using 13 mm pellets, prepared at a pressure of 200 MPa from mixtures of chromite (75–105 µm), graphite (25–37 µm, 22 or 28 wt % of ore), and ground anhydrous CaCl₂ (30 wt % of ore). It was later found by examining the reduced product that certain amounts of ferrochrome alloys were attached to the reduced chromite particles, due to the high pressure used in preparing the pellets. This created difficulties during the subsequent physical separation of ferrochrome alloys from the unwanted materials. A third test was therefore performed using the pellets containing 19 wt % graphite (i.e., stoichiometric amount), prepared with a much smaller pressure of approximately 0.7 MPa. All the 13 mm pellets used in the subsequent tests were prepared at a pressure of 0.7 MPa. The results from off-gas analysis with the temperature profiles are plotted in Figure 5 for comparison. As seen, the CO profiles for 22 and 28 wt % C are nearly identical, indicating that excessive graphite has little influence on the reduction rate. Comparatively, the pellets for the test using 19 wt % graphite were relatively loosely packed, because of a much smaller pressure used for pellet preparation. This would mean that larger gaps existed between the chromite and graphite particles. As a result, the reduction rate appeared slightly slower based on its CO profile. Cross sections of the products from reduction with 19 and 22 wt % graphite are illustrated in Figure 6. The residual chromite particles (grey) in Figure 6a contain on average 1.4 wt % Cr, and 0.1 wt % Fe based on the EDS microanalyses, translating to metallization degrees of 98.6 wt % Cr and 99.8 wt % Fe. The presence of residual graphite cores (black) in ferrochrome alloy particles (white) can be seen in Figure 6b, because of the excessive amount of graphite used. In comparison, reduction by the stoichiometric amount of carbon resulted in the formation of clean ferrochrome alloy particles that are free from inclusions of residual carbon, as seen in Figure 6a.

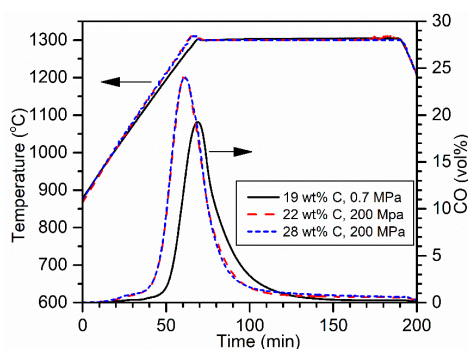


Figure 5. Temperature profiles and off-gas CO concentrations for the tests with the variation of graphite addition.

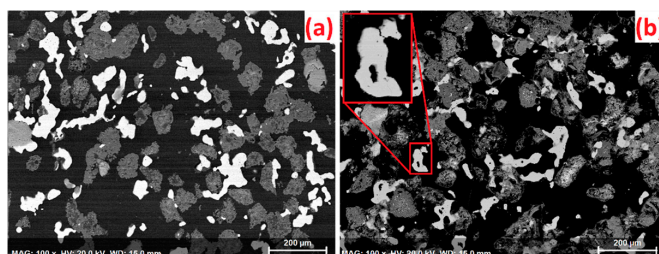


Figure 6. Backscattered electron micrographs of the products from reduction with (a) 19 wt % graphite and (b) 22 wt % graphite.

3.3. Effect of Reduction Temperature

Growth of ferrochrome alloy particles during the CaCl₂-assisted segregation reduction can be controlled by two main mechanisms. Firstly, the alloy particle size can be controlled by that of the graphite powders used for reduction because metallization takes place on graphite particles. Secondly,

sintering/coalescence of nearby alloy particles contributes further to the alloy growth, which can be promoted at a higher temperature. Therefore, a larger graphite particle size range was used in this study for the promotion of alloy growth.

Electric tube furnace reduction tests were performed on the 13 mm pellets composed of 10 g chromite (75–105 μm), graphite (75–105 μm , 22 wt % of ore), and anhydrous CaCl_2 powder (30 wt % of ore) to evaluate the influence of reduction temperature in the range of 1200–1400 $^\circ\text{C}$ (Figure 7). As the main gaseous reduction product at temperatures higher than 1000 $^\circ\text{C}$, CO concentration in the off-gas state directly relates to the reduction rate. As seen, the overall reduction was considerably slower at 1200 $^\circ\text{C}$. The reduction rate was comparably fast for 1300 and 1400 $^\circ\text{C}$, with near-complete reduction that took place within the first hour for both reduction temperatures. Figure 8 illustrates the cross sections and surface morphologies of the reduced product at 1200 $^\circ\text{C}$ and 1400 $^\circ\text{C}$. It should be noted that the samples for surface morphology observations were water-leached to remove chlorides, as indicated in the Section 2.5. As shown in Figure 8a, each chromite particle consists of an unreacted chromite core (light grey) surrounded by a partially reduced Cr-rich chromite rim (dark grey), based on EDS microanalysis. The presence of siliceous gangue minerals caused partial sintering among some chromite particles (e.g., the enlarged particles in Figure 8a). The chloride segregation effect resulted in the formation of ferrochrome metallic phase on the graphite particles, which appear as stripe-shaped white particles with unreacted graphite (black) core (Figure 8a), and as flake-shaped white particles (Figure 8b), which resemble the original shapes of the starting graphite particles. The ferrochrome alloy particles have an average Cr:Fe weight ratio of about 1.4:1, which is lower than that of the starting chromite (i.e., 2.0:1), indicating incomplete reduction of Cr. In comparison, carbothermic reduction at 1400 $^\circ\text{C}$ was complete and the high temperature resulted in substantial sintering among the ferrochrome alloy particles, contributing to the alloy growth (Figure 8c,d).

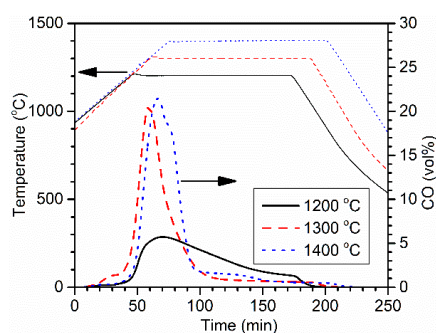


Figure 7. Temperature profiles and off-gas CO concentrations for the tests at different temperatures.

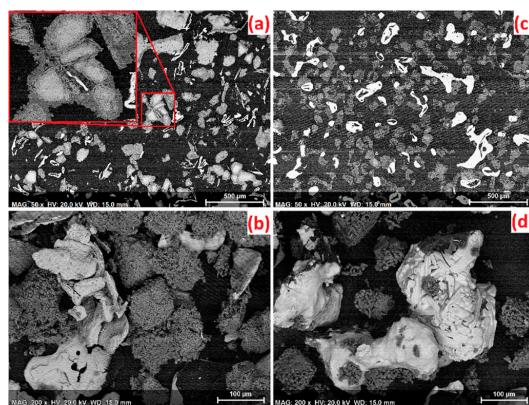


Figure 8. Backscattered electron micrographs of the products formed at 1200 $^\circ\text{C}$ (a,b), and 1400 $^\circ\text{C}$ (c,d). Photomicrographs (a,c) represent polished section surfaces while (b,d) show surface morphologies of the reduced products.

X-ray absorption spectra collected at the Fe K-edge indicate a significant reduction of Fe species at all the temperature ranges studied. The least-squares fitting of the measured spectra by a series of model compounds indicates metallization degrees of about 91.6% for the product formed at 1200 °C and 100% for the sample representing 1300 °C (Table 2). The simulated spectrum of 1200 °C sample does not adequately capture the measured oscillations at the extended range around 7185–7230 eV (Figure 9a), suggesting that the chromite and ferrochrome models are not representative of the Fe compounds present in the sample. It is likely that chromite is not present in the sample and that the degree of metallization is likely to be near 100% because the observed spectrum (especially the edge region) resembles both ferrochrome models shown (Figure 9a). The least squares fitting of the Cr K-edge X-ray absorption near edge structure (XANES) indicated that the samples are binary mixtures dominated by ferrochrome and lesser amounts of residual chromite (Table 2). The proportion of ferrochrome alloy indicates the degree of Cr metallization ranging from about 58.6% for the product formed at 1200 °C to 100% for the 1400 °C sample.

Table 2. Elemental distribution of Fe and Cr in the ferrochrome alloy and the residual chromite phases, produced from least-square fitting of the X-ray absorption spectra as shown in Figure 9.

Temperature (°C)	Elements	Ferrochrome (%)	Chromite (%)	χ^2 *
1200	Fe	91.6	8.4	0.014
	Cr	58.6	41.4	0.045
1300	Fe	100.0	0.0	0.067
	Cr	94.2	5.8	0.010
1400	Cr	100.0	0.0	0.211

* Chi square goodness of fit.

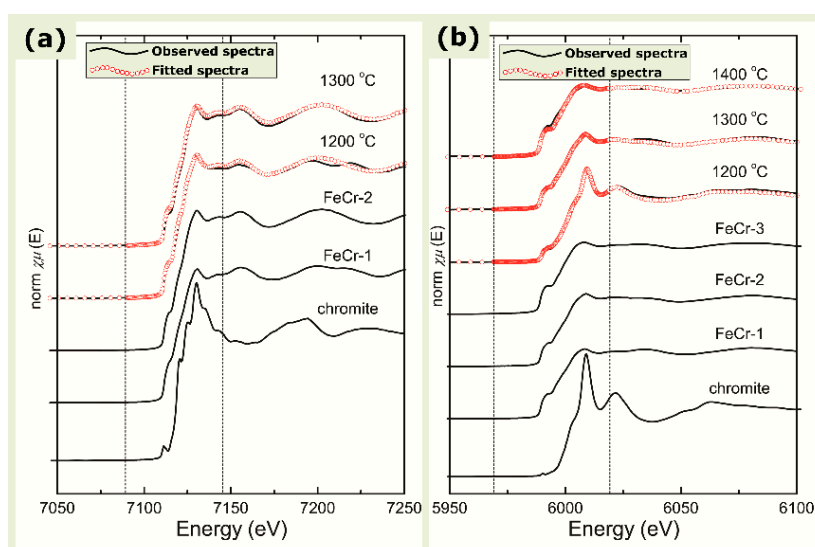


Figure 9. (a) Normalized Fe K-edge spectra of the products formed at 1200 and 1300 °C. Vertical dotted lines show the fitting range (i.e., 7092–7142 eV). Reference spectra used in least-squares fitting are shown for chromite (ore) and two Ring of Fire ferrochrome samples (FeCr-1 and FeCr-2); (b) Normalized Cr K-edge spectra of the products formed at 1200, 1300 and 1400 °C. The fitting range of 5970–6020 eV is marked by vertical dotted lines. Also shown are the spectra of the relevant model or reference compounds (chromite represents the starting ore material; FeCr-3 represents Cr_3C_2).

3.4. Effect of Chromite Particle Size

The influence of chromite particle size was evaluated with electric tube furnace reduction tests using 13 mm pellets prepared by mixing 10 g ore in the particle size ranges of 37–75 μm ,

105–180 μm and 180–300 μm) with 2.2 g graphite (105–150 μm), and ground 3 g anhydrous CaCl_2 . The mixtures were subjected to reduction at 1300 $^\circ\text{C}$ for 2 h (Figure 10). Strictly speaking, these reduction tests were influenced by a combination of both the chromite particle size and the amount of gangue minerals present in the starting ore because the ore with a smaller size fraction contained a higher proportion of the gangue minerals (as seen from Table 1 and Figure 1). To further assess the influence of the presence of gangue minerals, the reduced products were analyzed for their elemental compositions and were also leached with water to quantify the water-soluble species (Figure 11). The percentage of water-soluble species M was calculated based on Equation (2). As seen from Figure 10, a strong CO_2 peak appeared after about 20 min (500 $^\circ\text{C}$) when the ore sample in the 37–75 μm size fraction was reduced. This was caused by the thermal decomposition of magnesite present in the chromite ore, which can be represented by Equation (3). The corresponding CO_2 peak was insignificant for both the other two tests, as the chromite size fractions of 105–180 μm and 180–300 μm contained much less magnesite (Figure 1). The massive CO peaks appeared after 100 min were due to the carbothermic reduction of chromite. The CO profile for the 37–75 μm ore started at a lower temperature of approximately 1000 $^\circ\text{C}$, compared with the other two CO profiles. This was likely due to the presence of a much higher amount of siliceous gangue (e.g., clinocllore) in the 37–75 μm ore (Figure 1). Reaction between the molten CaCl_2 and the siliceous-gangue took place in the presence of residual moisture, leading to the formation of wadalite and gaseous HCl. With the presence of a relatively high partial pressure of HCl, chloride segregation and its induced carbothermic reduction of chromite became more effective at temperatures as low as 1000 $^\circ\text{C}$. Because of this, near-complete reduction of 37–75 μm chromite took place within the first hour at 1300 $^\circ\text{C}$ according to its CO profile. Another important promoting effect was the fact that a finer chromite particle size range was used in this test. Generally speaking, the reduction rate is less likely limited by the mass transfer within the chromite particles when finer chromite particles are used, in addition to the fact that greater specific surface areas are available for reduction.

$$\% \text{ water-soluble of M} = \frac{\text{Mass of M in water leachate}}{\text{Total mass of M in reduced product}} \times 100\% \quad (2)$$

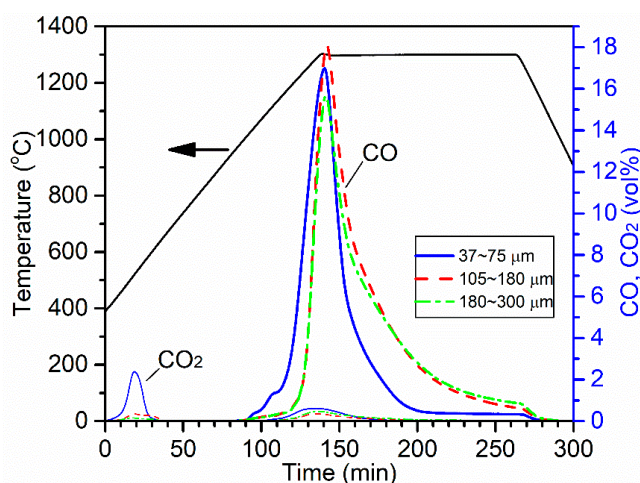


Figure 10. Temperature profiles, off-gas CO, and CO_2 concentrations for the tests with the variation of chromite particle size.

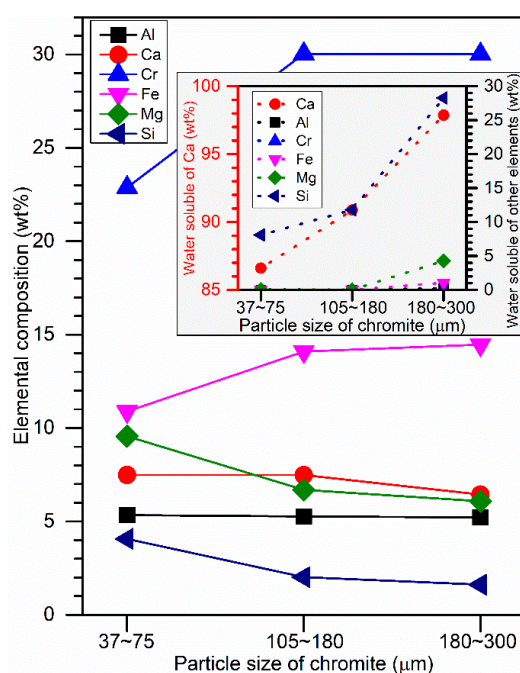


Figure 11. Elemental composition of the pellets reduced at 1300 °C, and the percentages of each element that are water-soluble (calculated based on Equation (2), and plotted as an inset).

In comparison, no appreciable reduction took place below 1200 °C when using 105–180 μm and 180–300 μm sized ore samples, because of much less siliceous-gangue present in both chromite fractions. The reduction also took longer time (~2 h) to reach near-complete reduction. The limited effect from the change of chromite particle size can be observed by comparing the two CO profiles for the 105–180 μm and 180–300 μm size fractions because a slightly higher CO peak can be seen from the use of 105–180 μm size fractions. Based on the analysis of the reduced products using synchrotron X-ray spectroscopy, Cr metallization of 100% was achieved for the test using 37–75 μm chromite fraction, while it was 98.9% for the 105–180 μm chromite fraction, and 75.8% for the 180–300 μm chromite fraction.

The results presented in Figure 11 confirmed the presence of higher amounts of gangue during the reduction of the 37–75 μm sample, as indicated by the higher concentrations of Si and Mg, and lower concentrations of Cr and Fe in the reduced product. Approximately 86.5 wt % Ca in this reduced product was water-soluble, presumably in the form of chloride. The remainder (13.5 wt %) was fixated as water-insoluble components (primarily as wadalite) from the reactions between CaCl₂ and the siliceous gangue. The percentage of water-soluble Ca became higher when the ore sample with the highest amount of chromite was used. For example, as much as ~98 wt % Ca in the reduced product was water-soluble when the sample with the highest amount of chromite (i.e., 180–300 μm) was reduced. It also should be noted that appreciable percentages of Si also became water-soluble, ranging from 8–28 wt %. This is because the silicate gangue was partially chloridized during reduction at high temperatures, leading to the formation of silicon chloride (SiCl₄), which existed possibly as both vapor and in dissolved form in the molten CaCl₂.

Figure 12 presents the cross sections in the reduced products, which clearly demonstrates the effective segregation in all three tests, forming discrete ferrochrome alloy particles. Due to the presence of higher amounts of gangue in the 37–75 μm size fraction, sintering among the chromite particles took place, evidenced by the irregular grey particles present in Figure 12a. A small fraction of the reduced chromite particles (dark grey) can be found to enclose a residual chromite core (light grey) in Figure 12c. One of the two such particles present in Figure 12c is shown in Figure 13, along with the EDS point microanalyses along the white arrow across the particle. A clear Fe concentration

gradient can be seen inside the chromite core, indicating the outward diffusion of Fe towards the oxide layer (the rim). Significant fluctuation of the elemental composition across the rim is due to the presence of finely-mixed multi-components (i.e., mono-oxide MgO, spinel, and chloride). It can also be observed that tiny Fe-rich alloy beads (white) were scattered in a confined zone surrounding the residual chromite core.

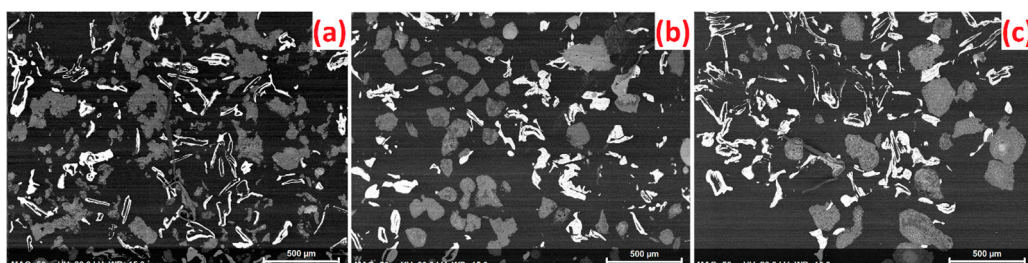


Figure 12. Backscattered electron micrographs of the reduced products resulted from the ore samples with particle size ranges of (a) 37–75 μm , (b) 105–180 μm , and (c) 180–300 μm .

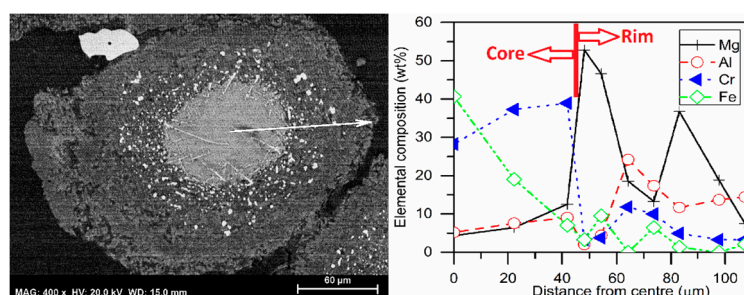


Figure 13. Cross section of a partially reduced chromite particle (180–300 μm) showing the residual chromite core (left); and the EDS elemental scan along the white arrow (right).

3.5. Influence of Pelletization

Agglomeration (e.g., pelletization, briquetting) of the powder feed is a common industrial practice in pyrometallurgical plants for various reasons, and requires some capital and operational costs. It was, therefore, reasonable to study the feasibility of directly treating the powder sample without agglomeration. Both 13 mm pellets and powders prepared from mixing chromite (37–75 μm), graphite (105–150 μm , 22 wt % of ore), and ground anhydrous CaCl_2 (30 wt % of ore), were subjected to reduction at 1300 $^\circ\text{C}$ for 2 h (Figure 14). As seen, the CO_2 peaks that appeared at about 40 min (500 $^\circ\text{C}$) were from the decomposition of magnesite as discussed earlier (Equation (3)). A comparatively lower and wider CO peak for the reduction of the powder sample revealed a slightly slower yet comparable reduction rate. This difference was mainly due to the loosely packed nature of the powder sample, meaning comparatively wider gaps existed between the chromite and the graphite particles. Segregation reduction involves transfer of reducible Cr and Fe as ionic species in the form of short polymeric species (i.e., monomers, dimers or trimers of Cr and Fe coordinated to O and/or Cl) from chromite to the surface of graphite where metallization takes place. The slower reduction rate when heating the powder sample implies that the reduction rate was determined or at least partially limited by the mass transfer between chromite and graphite particles. In addition to the reduction of chromite directly by solid carbon (Equation (1)), chromite can also be reduced by gaseous CO forming CO_2 (Equation (4)), resulting in the evolution of minor amounts of CO_2 at approximately 150 min when pellets were heated (Figure 14). The CO_2 can be further consumed by the Boudouard reaction, i.e., Equation (5). The absence of this minor CO_2 peak when the powder sample was used (Figure 14) strongly suggests that the Boudouard reaction was greatly promoted. Near-complete reduction was

achieved for both tests, indicated by both the EDS analysis on the reduced products, and the low off-gas CO concentration (<0.5 vol %) at the end of the two-hour dwell at 1300 °C. Analysis by synchrotron X-ray spectroscopy also suggests that 100% Cr metallization was achieved for both tests.

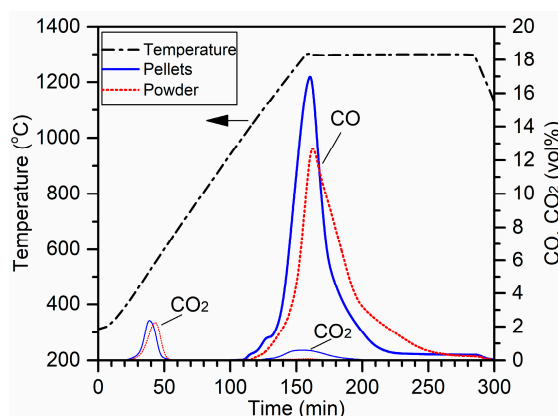


Figure 14. Temperature profiles, off-gas CO and CO₂ concentrations for the tests using pellet and powder samples.

Chemical analysis of the reduced products enabled mass balance calculations (Figure 15). This figure illustrates the redistribution of the four elements among the three components after reduction: (a) vaporized chlorides during reduction; (b) molten/condensed chlorides remaining in the reduced products, which is water-soluble; (c) gangue component, which is water-insoluble. It is obvious from this figure that the reduction of powder sample resulted in higher vapor losses in general, except for Al, which remained completely in the gangue. It is suggested that agglomeration (e.g., pelletization) is beneficial in terms of reducing the vapor loss, due to its closely-packed nature and lower porosity. As seen, approximately 9 wt % of the added CaCl₂ was consumed by reacting with siliceous gangue forming water-insoluble species (e.g., wadalite), as discussed earlier. About 60 wt % remained in the reduced products as chloride (i.e., Soluble), and 30 wt % evaporated during reduction, both of which can possibly be recovered as chloride for re-use from a practical point of view.

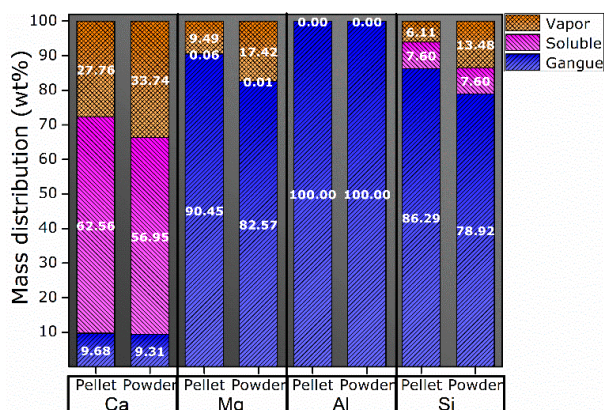


Figure 15. Mass distribution of the elements among three forms, i.e., Vapor: vaporized during reduction; Soluble: water-soluble form in the reduced product; Gangue: water-insoluble form in the reduced product.

3.6. Recovery of Ferrochrome

Approximately 170 g spherical pellets in the size range of 6.7–12.7 mm were produced using a laboratory disc pelletizer. These pellets were made from a mixture of chromite (75–105 μm), graphite (150–250 μm , 22 wt % of ore), and ground anhydrous CaCl_2 (30 wt % of ore), and were heated in an electrical tube furnace at 1300 $^\circ\text{C}$ for 3 h.

The reduced pellets were crushed gently and leached with water for the recovery of chloride. Solid CaCl_2 was successfully produced by boiling off water from the leachate. After drying in an oven, 10 g of the reduced powders was taken and subjected to sieving to produce five size fractions (Table 3). It was found that the size fraction of <105 μm was predominantly unwanted gangue with little-entrainment of alloy particles, and therefore can be rejected (as tailings in Table 3) without much metal loss. This was because the final alloy particle size was largely controlled by the starting graphite particle size (150–250 μm) due to the nature/mechanism of segregation reduction. As presented in Table 3, the other four size fractions were individually subjected to elutriating separation to produce (a) concentrate of alloy particles, (b) tailings composed largely of gangue particles, and (c) middlings which would require further processing. Figure 16 illustrates the surface morphologies of the three portions produced from elutriating separation of the 250–500 μm size fraction as an example. As seen, the concentrate fraction is composed essentially of ferrochrome alloy particles that are free of entrained gangue, whereas the tailings fraction contains little entrained alloy particles, demonstrating the effectiveness of the elutriating separation. Flake-shaped ferrochrome alloy particles (Figure 16a,b) resembling the original flake-shaped graphite powders used for the study further confirm the dominance of the segregation reduction mechanism in the presence of CaCl_2 . Therefore, to allow for reduction it is beneficial to use a larger particle size range of the graphite powders so that they are optimized for forming larger ferrochrome alloy particles allowing easier separation.

Table 3. Mass distribution (wt %) of the products in various size fractions following sieving-elutriating separation.

Size Fraction (μm)	Concentrate (wt %)	Middling (wt %)	Tailings (wt %)	Total (wt %)
>500	8.38	0	1.19	9.57
250–500	29.75	6.75	15.46	51.95
150–250	12.48	0.49	6.95	19.91
105–150	3.36	0	2.63	5.98
<105	0	0	12.58	12.58
Total	53.96	7.24	38.80	100

The elemental distribution of Cr, Fe, Mg, Al, and Si among the concentrate, middling, and tailings fractions is plotted in Figure 17, based on the chemical analysis. It should be noted that this concentrate fraction represents the combined concentrate produced from all size fractions. The same is true for the middling and tailings fractions. The concentrate fraction, representing 53.96 wt % of the total starting mass, contains impurities of 0.25 wt % Mg, 0.14 wt % Al, and 0.96 wt % Si in their oxide forms. This means the concentrate fraction has only 2.85 wt % oxides/silicates as the entrained gangue. As seen from Figure 17, metal recoveries of 83.5 wt % Cr and 90.6 wt % Fe were achieved in the concentrate fraction, while most of Mg, Al and Si reported to the Tailings fraction. The Middling fraction can be further processed to increase the metal recovery.

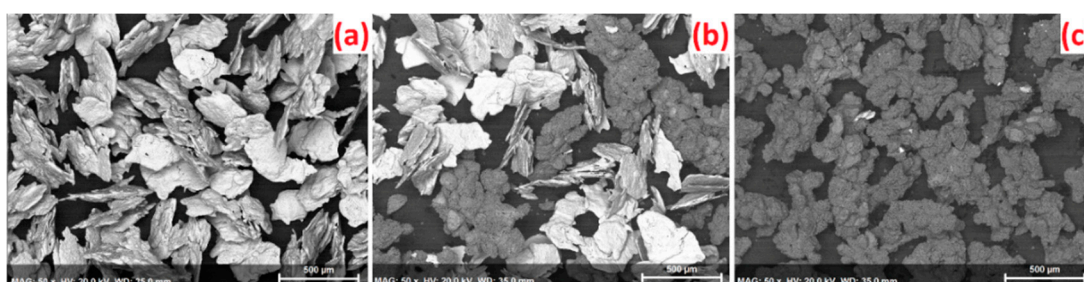


Figure 16. Backscattered electron micrographs of (a) concentrate, (b) middlings, and (c) tailings fractions produced from elutriating separation of the 250–500 µm size fraction of the reduced product. White or light grey particles are alloy whereas dark particles represent gangue.

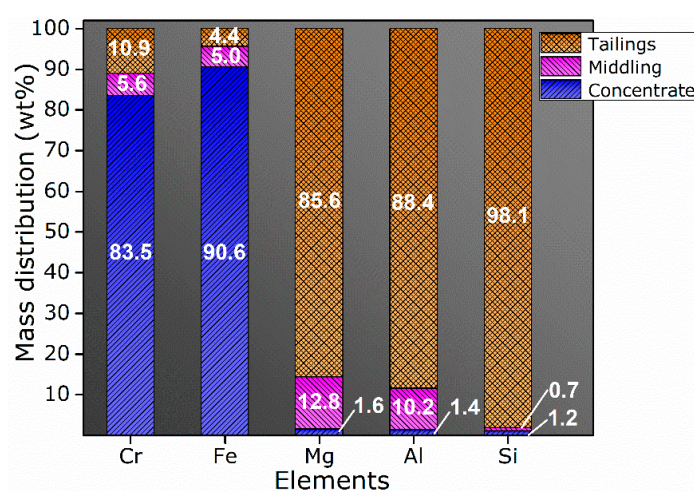


Figure 17. Elemental distribution (normalized to 100 wt % for each element) among the concentrate, middling, and tailings.

4. Conclusions

Addition of CaCl_2 was effective both in accelerating the carbothermic reduction of chromite and in promoting the formation of individual ferrochrome alloy particles from outside of the chromite particles via the chloride segregation mechanism. With the CaCl_2 additive, formation of finely divided alloy particles within chromite was minimized, which enabled the subsequent separation of ferrochrome from the unwanted gangue without the need of physical liberation (e.g., milling). The particle size of the alloys, which was largely determined by the particle size of the starting carbonaceous reductant (i.e., graphite), was large enough to allow efficient separation using the elutriating separation technique.

CaCl_2 -assisted carbothermic reduction of chromite by graphite was thermally activated and was relatively fast at temperatures higher than 1200 °C. Near-complete metallization of both Cr and Fe at 1300 °C generally took place between 1 to 2 h. Compared to the powder sample, pelletization of the mixture of chromite, graphite and CaCl_2 resulted in a slightly faster reduction. Pelletization minimized the evaporation of chloride during reduction because of its lower porosity. Only a stoichiometric amount of graphite was required for complete reduction. Excessive carbon addition resulted in the presence of residual carbon cores in the ferrochrome alloy particles. After segregation reduction, the residual chromite particles were highly porous and mainly composed of finely-divided monoxide (MgO) and spinel (MgAl_2O_4) phases. The presence of siliceous gangue (e.g., clinocllore) caused partial sintering among chromite particles during reduction, which also consumed CaCl_2 forming wadalite ($\text{Ca}_6\text{Al}_5\text{Si}_2\text{O}_{16}\text{Cl}_3$). The majority (~60%) of the CaCl_2 remained in the reduced product in a water-soluble chloride form, and about 30% evaporated during reduction. Both forms representing

>90% of the original CaCl_2 can be recovered for re-use to minimize the material cost from a practical point of view. By taking advantage of the density difference between the ferrochrome and the unwanted gangue, pure ferrochrome alloy (with 2.85 wt % gangue) in its M_7C_3 powder form was successfully produced using elutriating separation, with total metal recoveries of 83.5% Cr and 90.6% Fe.

Acknowledgments: The following contributions are acknowledged: Derek Smith for XRD analyses, Judith Price for the preparation of polished sections, and KWG Resources Inc. for providing the chromite ore samples. The study was funded by NRCan under the Rare Earth Elements and Chromite R&D Program. X-ray absorption experiments at the Advanced Photon Source were carried out under a General User Proposal to the senior author and a Partner User Proposal supported by the Natural Sciences and Engineering Research Council (NSERC) of Canada through a major facilities access grant. Research at the PNC-CAT beamline of APS, Argonne National Laboratory is supported by the U.S. Department of Energy under Contracts W-31-109-Eng-38 (APS) and DE-FG03-97ER45628 (PNC-CAT). We acknowledge the help provided by the beamline scientists Tianpin Wu and George Sterbinsky (9 BM) and Zou Finfrock (20 BM).

Author Contributions: Dawei Yu conceived and designed the experiments; Dawei Yu performed the experiments; Dawei Yu and Dogan Paktunc analyzed the data; Dawei Yu and Dogan Paktunc contributed reagents/materials/analysis tools; Dawei Yu and Dogan Paktunc wrote the paper.

Conflicts of Interest: The authors declare no conflict of interest.

References

1. Gasik, M.I. Technology of Chromium and Its Ferroalloys. In *Handbook of Ferroalloys: Theory and Technology*; Gasik, M., Ed.; Butterworth-Heinemann Elsevier: Oxford, UK, 2013; pp. 299–316, ISBN 9780080977539.
2. Curr, T.R. A review of new ferrochromium smelting technologies. Presented at the ICDA (International Chromium Development Association) Spring Meeting, Cape Town, South Africa, 11–13 March 1996; pp. 1–8.
3. Kapure, G.; Tathavadkar, V.; Rao, C.B.; Rao, S.M.; Raju, K.S. Coal based direct reduction of preoxidized chromite ore at high temperature. In Proceedings of the Twelfth International Ferroalloys Congress, Helsinki, Finland, 6–9 June 2010; pp. 293–302.
4. Johnson, J.; Reck, B.K.; Wang, T.; Graedel, T.E. The energy benefit of stainless steel recycling. *Energy Policy* **2008**, *36*, 181–192. [[CrossRef](#)]
5. Chakraborty, D.; Ranganathan, S.; Sinha, S.N. Investigations on the carbothermic reduction of chromite ores. *Metall. Mater. Trans. B* **2005**, *36B*, 437–444. [[CrossRef](#)]
6. Basson, J.; Daavittila, J. High Carbon Ferrochrome Technology. In *Handbook of Ferroalloys: Theory and Technology*; Gasik, M., Ed.; Butterworth-Heinemann Elsevier: Oxford, UK, 2013; pp. 317–363, ISBN 9780080977539.
7. Hill, R.J.; Craig, J.R.; Gibbs, G.V. Systematics of the spinel structure type. *Phys. Chem. Miner.* **1979**, *4*, 317–339. [[CrossRef](#)]
8. Yu, D.; Paktunc, D. Kinetics and Mechanisms of the Carbothermic Reduction of Chromite in the Presence of Nickel. *J. Therm. Anal. Calorim.* **2018**. [[CrossRef](#)]
9. Ding, Y.L.; Warner, N.A. Catalytic reduction of carbon-chromite composite pellets by lime. *Thermochim. Acta* **1997**, *292*, 85–94. [[CrossRef](#)]
10. Duong, H.V.; Johnston, R.F. Kinetics of solid state silica fluxed reduction of chromite with coal. *Ironmak. Steelmak.* **2000**, *27*, 202–206. [[CrossRef](#)]
11. Lekatou, A.; Walker, R.D. Effect of SiO_2 addition on solid state reduction of chromite concentrate. *Ironmak. Steelmak.* **1997**, *24*, 133–143.
12. Weber, P.; Eric, R.H. The reduction mechanism of chromite in the presence of a silica flux. *Metall. Trans. B* **1992**, *24*, 987–995. [[CrossRef](#)]
13. Weber, P.; Eric, R.H. Solid-state fluxed reduction of LG-6 chromite from the Bushveld complex. In *INFACON 6, Proceedings of the 6th International Ferroalloys Congress*; SAIMM: Cape Town, South Africa, 1992; pp. 71–77.
14. Weber, P.; Eric, R.H. The reduction of chromite in the presence of silica flux. *Miner. Eng.* **2006**, *19*, 318–324. [[CrossRef](#)]
15. Dawson, N.F.; Edwards, R.I. Factors affecting the reduction of chromite. In Proceedings of the 4th International Ferro-Alloys Congress, Sao Paulo, Brazil, 31 August–3 September 1986; pp. 105–113.
16. Dawson, N.F. The Solid State Reduction of Chromite. Ph.D. Thesis, Department of Chemical Engineering, University of Natal, Durban, South Africa, 1989.

17. Ding, Y.L.; Warner, N.A. Kinetics and mechanism of reduction of carbon-chromite composite pellets. *Ironmak. Steelmak.* **1997**, *24*, 224–229.
18. Kekkonen, M.; Xiao, Y.; Holappa, L. Kinetic study on solid state reduction of chromite pellets. In Proceedings of the INFACON, Trondheim, Norway, 11–14 June 1995; pp. 351–360.
19. Niayesh, M.J.; Dippenaar, R.J. The solid state reduction of chromite. In Proceedings of the INFACON 6, 6th International Ferroalloy Congress, Cape Town, South Africa, 8–11 March 1992; pp. 57–63.
20. Kekkonen, M.; Holappa, L.; Niemela, P. Kinetic study on smelting reduction of chromite ore. In Proceedings of the INFACON IX, The Ninth International Ferroalloys Congress, Quebec City, QC, Canada, 3–6 June 2001; pp. 157–165.
21. Soykan, O.; Eric, R.H.; King, R.P. The reduction mechanism of a natural chromite at 1416 °C. *Metall. Trans. B* **1991**, *22B*, 53–63. [[CrossRef](#)]
22. Moulden, J.C.; Taplin, B. Improvements in or Relating to the Heat Treatment of Oxidized Copper Ores. British Patent 250991, 1924.
23. Brittan, M.I. Kinetics of copper segregation by the Torco process. *J. S. Afr. Inst. Min. Metall.* **1970**, *70*, 278–289.
24. Kwatara, M.; Tayabally, J.; Peek, E.; Schonewille, R. Segregation roasting of a saprolitic ore—An experimental investigation. In *EPD Congress 2011*; Monteiro, S.N., Verhulst, D.E., Anyalebechi, P.N., Pomykala, J.A., Eds.; John Wiley & Sons, Inc.: Hoboken, NJ, USA, 2011.
25. Mehrotra, S.P.; Srinivasan, V. Extraction of nickel from an Indian laterite by segregation roasting. *Trans. Inst. Min. Metall.* **1994**, *103*, C97–C104.
26. Zhou, S.; Wei, Y.; Li, B.; Wang, H.; Ma, B.; Wang, C. Chloridization and reduction roasting of high-magnesium low-nickel oxide ore followed by magnetic separation to enrich ferronickel concentrate. *Metall. Mater. Trans. B* **2016**, *47B*, 145–153. [[CrossRef](#)]
27. Bhattacharya, M. Reaction mechanism and thermodynamics of segregation roasting of iron oxide. *Int. J. Miner. Process. Extr. Metall.* **2016**, *1*, 64–69.
28. Hernandez, V.; Peake, K.; Dalvi, A.; Brown, R.; Olurin, J.; O'Farrell, T.; Zhou, M.; Liu, B.; Cameron, I. Process development of a new DRI technology for Oolitic iron ores. In *AISTech Proceedings*; Association for Iron & Steel Technology: Pittsburgh, PA, USA, 2013; pp. 519–526.
29. Gruszkiewicz, M.S.; Simonson, J.M. Vapor pressures and isopiestic molalities of concentrated CaCl₂(aq), CaBr₂(aq), and NaCl(aq) to T = 523 K. *J. Chem. Thermodyn.* **2005**, *37*, 906–930. [[CrossRef](#)]
30. Sharma, S.D.; Kitano, H.; Sagara, K. *Phase Change Materials for Low Temperature Solar Thermal Applications*; Research Reports of the Faculty of Engineering; Mie University: Mie, Japan, 2004; Volume 29, pp. 31–64.
31. N'Tsoukpoe, K.E.; Rammelberg, H.U.; Lele, A.F.; Korhammer, K.; Watts, B.A.; Schmidt, T.; Ruck, W.K.L. A review on the use of calcium chloride in applied thermal engineering. *Appl. Therm. Eng.* **2015**, *75*, 513–531. [[CrossRef](#)]
32. Lide, D.R. *CRC Handbook of Chemistry and Physics*, 90th ed.; CRC Press: Boca Raton, FL, USA, 2009.
33. Frost, I.C. An elutriating tube for the specific gravity separation of minerals. *Am. Miner.* **1959**, *44*, 886–890.
34. Ravel, B.; Newville, M. ATHENA, ARTEMIS, HEPHAESTUS: Data analysis for X-ray absorption spectroscopy using IFEFFIT. *J. Synchrotron Radiat.* **2005**, *12*, 537–541. [[CrossRef](#)] [[PubMed](#)]



© 2018 by the authors. Licensee MDPI, Basel, Switzerland. This article is an open access article distributed under the terms and conditions of the Creative Commons Attribution (CC BY) license (<http://creativecommons.org/licenses/by/4.0/>).